

Image of a subsurface current core in the southern South China Sea

Qunshu Tang¹, Dongxiao Wang², Jiabiao Li³, Pin Yan¹, Jian Li²

[1]{Key Laboratory of Marginal Sea Geology, South China Sea Institute of Oceanology, Chinese Academy of Sciences, Guangzhou 510301, China }

[2]{State Key Laboratory of Tropical Oceanography, South China Sea Institute of Oceanology, Chinese Academy of Sciences, Guangzhou 510301, China }

[3]{Key Laboratory of Submarine Geoscience, Second Institute of Oceanography, State Oceanic Administration, Hangzhou, China }

Correspondence to: Dongxiao Wang (dxwang@scsio.ac.cn)

Abstract

A legacy seismic transect acquired on 30 and 31 May 2009 in the southern South China Sea (SCS) was reprocessed to reveal the thermohaline structure of the water column. In the study region, a mesoscale subsurface lens with extraordinary features was detected at (113.5°E, 11.5°N). It is centered at 450 m depth, occupies both the subsurface and intermediate water from 250 to 600 m, and has a diameter of around 60 km. The simulated results from Hybrid Coordinate Ocean Model reveal an eddy-induced subsurface current running southwestward along the deep basin edge and suggest that the imaged lens is a snapshot of the subsurface current core rather than a subsurface eddy.

1 Introduction

A subsurface current (or undercurrent) is a type of current that runs below the ocean surface. Geographically, three main classes of undercurrents are often concerned: the Equatorial Undercurrents, the Western Boundary Undercurrents, and the Eastern Boundary Undercurrents (e.g., Lindstrom et al., 1987; Qu et al., 1997; Pierce et al., 2000; Montes et al., 2010). Like the current systems at the ocean surface, these subsurface currents also play an

1 irreplaceable role in the ocean circulation, transport, mixing, and ecosystem. Since no
2 extensive spatial observations, such as the satellite images, can be obtained, the subsurface
3 currents are less understood.

4 Recently, a new ocean observation technique, Seismic Oceanography, has been used to image
5 the structures in the ocean interior with a high lateral resolution of $O(10\text{ m})$ (e.g., Holbrook et
6 al., 2003). Theoretically, a seismic image shows the derivative of acoustic impedance
7 (product of density and velocity) of the water. Essentially, it is a smoothed map of vertical
8 temperature gradient (Ruddick et al., 2009). Various oceanic phenomena, such as fronts,
9 currents, boundaries, eddies, internal waves/tides, etc., have been successfully imaged in the
10 global ocean (e.g., Holbrook and Fer, 2005; Holbrook et al., 2009; Ruddick et al., 2009; Tang
11 and Zheng, 2011). Take the oceanic currents (surface and subsurface) for example, the
12 seismic image can easily capture the weak differences between two water masses, and then
13 confine the currents exactly from the reflective fronts or boundaries (e.g., Holbrook et al.,
14 2003; Nandi et al., 2004; Nakamura et al., 2006; Buffett et al., 2009; Pinheiro et al., 2010;
15 Quentel et al., 2010; Tang and Zheng, 2011; Vsemirnova et al., 2012).

16 The South China Sea (SCS) is the largest semi-enclosed marginal sea in the Northwest Pacific.
17 The upper-layer circulation of the SCS is mainly driven by the monsoon, with significant
18 influence from the Kuroshio in the northern SCS (Qu, 2000). Its multi-eddy structure has been
19 examined by numerous studies using traditional methods (e.g., Wang et al., 2003; Xiu et al.,
20 2010; Nan et al., 2011). In contrast, as a cul-de-sac of the North Pacific Intermediate Water
21 (NPIW), the SCS' intermediate layer circulation and mesoscale structures are seldom
22 documented (e.g., Isobe and Namba, 2001; You et al., 2005; Xie et al., 2011). Numerical
23 results by You et al. (2005) showed that the intermediate circulation is cyclonic in
24 winter/spring and anticyclonic in summer/fall. The monsoon is also the primary forcing of the
25 intermediate circulation. Observation data revealed a southward-verging wedge of the low
26 salinity anomaly between 400-700 m depth, indicating a southward spreading path of the
27 NPIW (Wang et al., 2004). Xie et al. (2011) reported an anticyclonic eddy in the intermediate
28 layer (500–900 m) of the Luzon Strait, which might be generated by both baroclinic
29 instability and the interaction of the current with the bottom topography, rather than by the
30 Kuroshio or the surface wind.

31 Mesoscale activities are also pervasive in the southern SCS (Fig. 1) because of the strong
32 monsoon and rough topography. In the area, the circulation in summer is often characterized

by a dipole flow pattern, in which a separated coastal jet (i.e., the Southeast Vietnam Offshore Current, SEVOC) is sandwiched by an anticyclonic circulation to the south and a cyclonic circulation to the north (Wang et al., 2006; Gan and Qu, 2008). Observational data shows that the vertical extent of the separated coastal jet is more than 300 m (Fang et al., 2002). A diagnostic calculation shows that the coastal jet is shallower than 500 m, while the anticyclonic eddy reaches deeper than 500 m (Wang et al., 2004). Hu et al. (2011) studied the three-dimensional structure of the north part of the dipole, and found that the eddy extended downward for more than 250 m with a vertically heterogeneous structure. Although some studies suggested deep penetration of these eddies to the subsurface and intermediate layers in the SCS, most studies have referred them as upper-layer-dominated features.

In this paper, we report a subsurface lens-like structure captured by a seismic survey in the southern SCS (113.5°E, 11.5°N) at the end of spring. Approximately, it was centred at 450 m depth, extending from 250 m to 600 m depth with a diameter of ~60 km. Generally, such structures may be considered as the subsurface eddies without further constraints (e.g., Sheen et al., 2009; Huang et al., 2010). However, the high-resolution velocity field simulated from a global Hybrid Coordinate Ocean Model (HYCOM) suggests that the lens-like structure is more like a cross-section of a subsurface current/flow, rather than an subsurface eddy described by Huang et al. (2010).

2 Data

From 30 May to 1 June 2009, a seismic survey line labelled NH973–01B was carried out by the Guangzhou Marine Geological Survey of the Chinese Ministry of Land and Resources. The line traversed from the southwestern basin to the Spratly Islands region, with a vessel heading of 161° (Fig. 1). Because of the strong streamer feathering (Max. 12.5°) during the data acquisition, the line was divided into two parts: the north and the south subsections, with a time gap of approximately 5 hours from 4:01 to 9:17 on 31 May 2009 at the line junction. The source was composed of 4 arrays of BOLT guns (total volume of 83 litres) that were triggered every 37.5 m. The data were collected using a 480-channel streamer with 250-m near-offset and 12.5-m channel spacing. The record length was 12 s with a sampling rate of 2 ms. In the present study, 120 near-source traces and the first 4 s of the data were sampled for imaging.

The data processing procedure is similar to that in Tang and Zheng (2011). One exception is that a two-layer velocity model was used during the pre-stack depth migration: 1510 m/s above 360 m and 1480 m/s below this depth, simplified from the CTD measurements by Nan et al. (2011). Our migration tests have shown that it is an acceptable velocity model.


As a common defect for the legacy seismic data, we have no in-situ hydrographic data to directly support the seismic observation. Since the subsurface structures could also have considerable influence on the ocean surface that could be detected from space (Oliveira et al., 2000; Takikawa et al., 2005), the satellite altimetry data of sea surface anomaly (SLA) and their by-products of geostrophic currents produced by the AVISO are presented. Meanwhile, the daily outputs of the HYCOM, which is an eddy-resolving ($1/12^\circ$ equatorial resolution) assimilated ocean circulation model, provide convincing evidences to further study the regional mesoscale activities for the period of cruise. Vertically, the simulated HYCOM current structure above 600 km depth is reliable according to the previous studies (Adams et al., 2011; Xie et al., 2011).


3 Results

Figure 2 shows the final migration result of the seismic profile. The upper (lower) panel is the north (south) subsection. Generally, the thermohaline reflections along the profile can be clearly recognized above 800-m depth. Further, this informative reflection zone can be divided into two layers around 300 m depth: strong reflection layer above and moderate-to-weak reflection layer below, corresponding to the upper and intermediate water layers, respectively. The noises dominate the profile below 800 m and reflections are nearly blanking (not shown below 900 m), a strong indicative of the deep water. This division by seismic reflection is very similar to the hydrographic observations (e.g., Li et al., 2002; Wang et al., 2004; You et al., 2005).


On the seismic image, the overall continuity of the finescale thermohaline reflections is poor, especially around the central part of the north subsection where strong intermittency occurs. This phenomenon indicates weak or disrupted stratification, probably caused by strong mixing. Internal waves are weakly developed, characterized by small vertical undulations of 10 m, typically weaker than the internal waves at the northeastern SCS and Luzon Strait (Dong et al., 2009; Tang and Zheng, 2011). In addition, it seems that the vertical undulations

of the internal waves in the north (deep basin region) are even weaker than those in the south (shallower multi-island region) along the transect. Both appearances support that the topography is an important factor for the generation and development of internal waves.

Further, three prominent mesoscale anomalies can be recognized from the seismic image: (1) a relatively strong reflection zone down to ~600 m at the beginning of the north subsection (ca. 0– m), (2) a lens-like structure centred at ~450 m at the end of the north subsection (ca. 170–220 km), and (3) a narrow, north-dipping zone with strong reflection down to ~350 m around two-thirds of the south subsection (ca. 380–400 km). Among them, the lens-like structure is the most striking and appealing phenomenon along the transect. Its detailed structure is redrawn in Fig. 3. It should be emphasized that this subsurface lens has been firstly mentioned briefly by Huang et al. (2010). No similar subsurface structure has been reported in the southern SCS by hydrographic observations so far.

Located at (113.5°E, 11.5°N) and centred at 450 m, the lens-like structure occupies both subsurface and intermediate water from ~250 to 600 m (Fig. 3). The right periphery of the structure is missing because of the temporal termination of the seismic transect. Although the south subsection is sequential spatially with the north subsection, a time gap of 5 hours has caused the seismic reflections untraceable, indicating a quick variation of the water column. From the present shape of the captured part (~50 km) of the lens, however, a diameter of ~60 km can be estimated .

4 Discussions

Although the lens-like structure is clearly traceable from the seismic image, the overall reflection features between the lens-like structure and the lateral background acoustic structure are not distinct, implication of weak difference of the thermohaline structure between them. A chaotic zone along the north periphery of the lens, which is less well developed than Meddies, is suggestive of xing zone. The reflection of the dome-shaped upper edge is extremely strong and continuous. The lower edge is also characterized by high reflectivity, which is typically deeper extended than the surrounding regions and comparable to the mesoscale anomaly at the beginning of the north subsection mentioned above. The low reflectivity of the core is suggestive of homogeneous water relatively. To an extent, these reflection features of the lens are similar to some of the Meddies (e.g., Biescas et al., 2008;

Pinheiro et al., 2010). Huang et al. (2010) believed that this is a representative vertical structure of an eddy. Nevertheless, we need more evidences to show whether or not the lens-like structure is a subsurface eddy. If not, which oceanic phenomenon will be responsible for the imaged mesoscale structure.

On the SLA map (Fig. 4a), we can see that the north subsection of the seismic line is located in a positive SLA region with two peaks higher than 12 cm. The imaged lens structure is located between the southwest flank of the south peak and the northeast of the SEVOC, surrounded by a weak anticyclonic eddy and a strong northwestward geostrophic current derived from the SLA. Here, the resolution of the SLA is acceptable because of the high consistency between the SLA-derived geostrophic currents and the in-situ records of the streamer feathering (Fig. 4b). Considering that the subsurface eddies can have a surface signature in SLA map sometimes (Oliveira et al., 2000; Takikawa et al., 2005), it seems ideal that the imaged lens structure is interpreted as a vertical snapshot of a subsurface eddy.

However, the simulated 3D results from HYCOM on 30 May 2009 do not support such an assumption which is inferred just from the surface appearance of SLA. Figure 5 shows the velocity fields and their corresponding streamlines at 50m, 100 m, 300 m and 600 m depth. The current speeds and velocities along the seismic transect are also presented in Fig. 6. At shallow depth, the satellite derived SLA and currents, the in-situ observed streamer feathering, and the simulated velocities (Figs. 4-6) are quite consistent. At 50 m and 100 m depth (Fig. 5a,b) near the north subsection, we can see that an anticyclonic eddy corresponds well to the north peak of the positive SLA, and gradually deviates from the south peak of the positive SLA with increasing depth. The vertical depth of the eddy with current speed larger than 5 cm/s is shallower than 150 m typically (Fig. 6a). Thus we believe that the strong baroclinic surface eddy is responsible for the positive SLA rather than the mesoscale anomalies in the subsurface layer. Meanwhile, the vertical extent of the energetic SEVOC mean flow is also shallower than 150 m during its juvenile stage (Figs. 5b and 6). This simulated result is reliable in that the observation of the SEVOC related eddy is shallower than 300 m even during the mature stage (Hu et al., 2011). Thus, a possibility that the imaged lens structure was caused from the strong baroclinic surface current of SEVOC by means of frontal instability, shedding, or flow-topography interaction can be also rejected substantially. In addition, hydrographic observations have shown that the subsurface eddy in the SCS cannot be generated by a Meddy-like generation mechanism, i.e., advected by the inflow of the

1 Pacific intermediate water (e.g., North Pacific Intermediate Water, Antarctic Intermediate
2 Water). Though evidence does exist to suggest that the Pacific intermediate water can intrude
3 into the South China Sea via the Luzon Strait, the water's low-salinity and high-oxygen
4 characteristics are not detectable in the southern part of the basin due to enhanced mixing (Qu
5 and Lindstrom, 2004; You et al., 2005).

6 On the contrary, there is a unique prominent feature of the HYCOM simulated velocities
7 between 200 m to 700 depth (Figs. 5c,d and 6) that a southwest current flows along the deep
8 basin edge of the SCS. The seismic transect just cut across the current obliquely. The widest
9 and strongest current flow is at 300 m depth and centred at 200 km distance of the transect.
10 From top to bottom, both widths and speeds of the current core is decreased gradually from ~
11 200 km to 100 km and ~ 15 cm/s to 5 cm/s, respectively. Obviously, the location of the
12 simulated current core matches perfectly well to the imaged subsurface lens. Further, the
13 upward bowing of the simulated isotherms (not shown) are also consistent with the reflections
14 of the lens structure generally. This appearance of the isotherms bending is suggestive of the
15 geostrophic adjustment of a subsurface current (Wang, 2005). In view of no vortex velocities
16 simulated near the study region, we believe that the imaged lens-like structure is the snapshot
17 of a southwestward current core as simulated. This subsurface current carries the nearby water
18 slowly (~ 10 km per day) to the study region and thus a lens-shaped current core is captured
19 in spite of the weak thermohaline contrast.

20 Figure 7 shows the daily speeds of the HYCOM results along the transect from 28 May to 2
21 June 2009. It is clearly seen that strength of the simulated subsurface current is intermittent
22 temporally. From 30 to 31 May 2009 (Fig. 7c,d), the strength of the subsurface current
23 weakens dramatically. As aforementioned, the 5-hour time gap at the line junction has caused
24 the reflections untraceable, which is a strong indication of a quick water column variation.
25 Therefore, there is a good agreement between the seismic observation and the simulated result
26 on the temporal variation of the water column. The missing right periphery of the subsurface
27 lens might be a result of a weakened current.

28 Considering that the 3D subsurface current simulated by HYCOM and the imaged subsurface
29 lens by seismic reflection are perfectly consistent both spatially and temporally, it is more
30 acceptable to interpret the subsurface lens as a current core, rather than a subsurface eddy.
31 The remain question is, what is the cause of the subsurface current along the deep basin edge?
32 The 3D current velocities in Fig. 5 shows that an energetic cyclonic-anticyclonic eddy pair

dominates the central basin of the SCS. The upstream of the subsurface current is separated from the divergent point of the eddy pair. Therefore, we considered that an eddy-induced current flows southward, turns southwestward and narrows down modified by both geostrophic effects and topography, and then runs straightforward along the deep basin edge, is the highly possible process of the subsurface current. In this process, the factors like vertical extent, lateral size, and strength of the eddy pair must have played important roles in the subsurface current forming, as well as the topography effects during the current marching. A preliminary census of the simulated velocity fields in the study region suggests that the subsurface currents are pervasive and the topography effect might be very important. Numerical tests would be useful to assess these factors quantitatively, but beyond the scope of this work.

5 Conclusions

A legacy seismic line acquired from 30 May to 1 June 2009 in the southern SCS was reprocessed to reveal the thermohaline structure of the water column. Similar to a previous study in the northeast SCS by Tang and Zheng (2011), the water column can be divided into three layers: (1) upper layer, above ~300 m with strong reflections; (2) intermediate layer, between 800–300 m with moderate-to-weak reflections; and (3) deep layer, below ~800 m characterized by acoustic blanking. However, the finescale features are quite different from those in the northern SCS. The reflections are intermittent all along the profile. Internal waves are weakly developed with vertical undulations of only 5–10 m.

The most interesting feature is the mesoscale subsurface lens located at (113.5°E, 11.5°N). It is centred at 450 m, occupies both the subsurface and intermediate water from 250 to 600 m, and has a diameter of ~60 km. Simulated results from HYCOM reveal an eddy-induced subsurface current flowing southwestward along the deep basin edge and suggest that the subsurface lens is a snapshot of the current core rather than a subsurface eddy. It could be misleading while the altimetric maps are used to be related to the subsurface structures.

This study gives new insight into the dynamic processes of the subsurface and intermediate water in the SCS. The subsurface currents in the study region are pervasive but transient and affect only a small area. To quantitatively assess the factors that control the formation and evolution of the subsurface currents in the southern SCS will be an interesting work.

1

2 **Acknowledgements**

3 We thank the *R/V Tanbao* crew for the seismic data acquisition. We thank Professor
4 Tangdong Qu for his helpful discussions. The altimeter products were produced by
5 Ssalto/Duacs and distributed by the AVISO, with support from the CNES
6 (www.aviso.oceanobs.com/duacs). The HYCOM data are available from
7 <http://hycom.org/dataserver>. This research is supported financially by the National Natural
8 Science Foundation of China (Grants 41176026 and 40904011) and the National Basic
9 Research Program of China (973 Program , Grant 2007CB411706).

10

References

- Adams, D. K., McGillicuddy, D. J., Zamudio, L., Thurnherr, A. M., Liang, X. F., Rouxel, O., German, C. R., and Mullineaux, L. S.: Surface-Generated Mesoscale Eddies Transport Deep-Sea Products from Hydrothermal Vents, *Science*, 332, 580-583, 10.1126/science.1201066, 2011.
- Biescas, B., Sallares, V., Pelegri, J. L., Machin, F., Carbonell, R., Buffett, G., Danobeitia, J. J., and Calahorrano, A.: Imaging meddy finestructure using multichannel seismic reflection data, *Geophys. Res. Lett.*, 35, L11609, 10.1029/2008gl033971, 2008.
- Buffett, G. G., Biescas, B., Pelegri, J. L., Machin, F., Sallares, V., Carbonell, R., Klaeschen, D., and Hobbs, R.: Seismic reflection along the path of the Mediterranean Undercurrent, *Cont. Shelf Res.*, 29, 1848-1860, 10.1016/j.csr.2009.05.017, 2009.
- Dong, C. Z., Song, H. B., Hao, T. Y., Chen, L., and Song, Y.: Studying of oceanic internal wave spectra in the Northeast South China Sea from seismic reflections, *Chin. J. Geophys.*, 52, 2050-2055 (in Chinese), 2009.
- Fang, W. D., Fang, G. H., Shi, P., Huang, Q. Z., and Xie, Q.: Seasonal structures of upper layer circulation in the southern South China Sea from in situ observations, *J. Geophys. Res.*, 107, 3202, 10.1029/2002jc001343, 2002.
- Gan, J., and Qu, T.: Coastal jet separation and associated flow variability in the southwest South China Sea, *Deep-Sea Res Pt I*, 55, 1-19, 10.1016/j.dsr.2007.09.008, 2008.
- Holbrook, W. S., Paramo, P., Pearse, S., and Schmitt, R. W.: Thermohaline fine structure in an oceanographic front from seismic reflection profiling, *Science*, 301, 821-824, 2003.
- Holbrook, W. S., and Fer, I.: Ocean internal wave spectra inferred from seismic reflection transects, *Geophys. Res. Lett.*, 32, L15604, 10.1029/2005gl023733, 2005.
- Holbrook, W. S., Fer, I., and Schmitt, R. W.: Images of internal tides near the Norwegian continental slope, *Geophys. Res. Lett.*, 36, L00D10, 10.1029/2009gl038909, 2009.
- Hu, J. Y., Gan, J. P., Sun, Z. Y., Zhu, J., and Dai, M. H.: Observed three-dimensional structure of a cold eddy in the southwestern South China Sea, *J. Geophys. Res.*, 116, C05016, 10.1029/2010jc006810, 2011.

- 1 Huang, X. H., Song, H. B., Dong, C. Z., and Bai, Y.: Seismic oceanography research on the
2 eddy and water movement in the South China Sea, The Chinese Geophysics, 26th annual
3 meeting of Chinese Geophysics Society, Ningbo, China, abstract #52, 2010.
- 4 Isobe, A., and Namba, T.: The circulation in the upper and intermediate layers of the South
5 China Sea, *J. Oceanogr.*, 57, 93-104, 2001.
- 6 Li, F. Q., Li, L., Wang, X. Q., and Liu, C. L.: Water masses in the South China Sea and water
7 exchange between the Pacific and the South China Sea, *Journal of Ocean University of*
8 *Qingdao*, 1, 19-24, 2002.
- 9 Lindstrom, E., Lukas, R., Fine, R., Firing, E., Godfrey, S., Meyers, G., and Tsuchiya, M.: The
10 Western Equatorial Pacific-Ocean Circulation Study, *Nature*, 330, 533-537, 1987.
- 11 Montes, I., Colas, F., Capet, X., and Schneider, W.: On the pathways of the equatorial
12 subsurface currents in the eastern equatorial Pacific and their contributions to the Peru-Chile
13 Undercurrent, *J Geophys Res-Oceans*, 115, C09003, 10.1029/2009jc005710, 2010.
- 14 Nakamura, Y., Noguchi, T., Tsuji, T., Itoh, S., Niino, H., and Matsuoka, T.: Simultaneous
15 seismic reflection and physical oceanographic observations of oceanic fine structure in the
16 Kuroshio extension front, *Geophys. Res. Lett.*, 33, L23605, 10.1029/2006gl027437, 2006.
- 17 Nan, F., He, Z. G., Zhou, H., and Wang, D. X.: Three long-lived anticyclonic eddies in the
18 northern South China Sea, *J. Geophys. Res.*, 116, C05002, 10.1029/2010jc006790, 2011.
- 19 Nandi, P., Holbrook, W. S., Pearse, S., Paramo, P., and Schmitt, R. W.: Seismic reflection
20 imaging of water mass boundaries in the Norwegian Sea, *Geophys. Res. Lett.*, 31, L23311,
21 10.1029/2004gl021325, 2004.
- 22 Pierce, S. D., Smith, R. L., Kosro, P. M., Barth, J. A., and Wilson, C. D.: Continuity of the
23 poleward undercurrent along the eastern boundary of the mid-latitude north Pacific, *Deep-Sea*
24 *Res Pt II*, 47, 811-829, 2000.
- 25 Pinheiro, L. M., Song, H. B., Ruddick, B., Dubert, J., Ambar, I., Mustafa, K., and Bezerra, R.:
26 Detailed 2-D imaging of the Mediterranean outflow and meddies off W Iberia from
27 multichannel seismic data, *J. Mar. Sys.*, 79, 89-100, 10.1016/j.jmarsys.2009.07.004, 2010.
- 28 Qu, T. D., Kagimoto, T., and Yamagata, T.: A subsurface countercurrent along the east coast
29 of Luzon, *Deep Sea Res. Part I*, 44, 413-423, 1997.

1 Qu, T. D.: Upper-layer circulation in the South China Sea, *J. Phys. Oceanogr.*, 30, 1450-1460,
2 2000.

3 Qu, T. D., and Lindstrom, E. J.: Northward intrusion of Antarctic intermediate water in the
4 western Pacific, *J. Phys. Oceanogr.*, 34, 2104-2118, 2004.

5 Quentel, E., Carton, X., Gutscher, M. A., and Hobbs, R.: Detecting and characterizing
6 mesoscale and submesoscale structures of Mediterranean water from joint seismic and
7 hydrographic measurements in the Gulf of Cadiz, *Geophys. Res. Lett.*, 37, L06604,
8 10.1029/2010gl042766, 2010.

9 Ruddick, B., Song, H. B., Dong, C. Z., and Pinheiro, L.: Water column seismic images as
10 maps of temperature gradient, *Oceanography*, 22, 192-205, 2009.

11 Sheen, K. L., White, N. J., and Hobbs, R. W.: Estimating mixing rates from seismic images of
12 oceanic structure, *Geophys. Res. Lett.*, 36, L00D04, 10.1029/2009gl040106, 2009.

13 Takikawa, T., Ichikawa, H., Ichikawa, K., and Kawai, S.: Extraordinary subsurface
14 mesoscale eddy detected in the southeast of Okinawa in February 2002, *Geophys. Res. Lett.*,
15 32, L17602, 10.1029/2005gl023842, 2005.

16 Tang, Q. S., and Zheng, C.: Thermohaline structures across the Luzon Strait from seismic
17 reflection data, *Dyn. Atmos. Oceans*, 51, 99-113, 10.1016/j.dynatmoce.2011.02.001, 2011.

18 Vsemirnova, E. A., Hobbs, R. W., and Hosegood, P.: Mapping turbidity layers using seismic
19 oceanography methods, *Ocean Sci.*, 8, 11-18, 10.5194/Os-8-11-2012, 2012.

20 Wang, C. Z.: Subthermocline tropical cells and equatorial subsurface countercurrents, *Deep-*
21 *Sea Res Pt I*, 52, 123-135, 10.1016/j.dsr.2004.08.009, 2005.

22 Wang, D. X., Chen, J., Chen, R. Y., Zhu, B. C., Guo, X. G., Xu, J. D., and Wu, R. S.:
23 Hydrographic and circulation characteristics in middle and southern South China sea in
24 summer, 2000, *Oceanologia et Limnologia Sinica*, 35, 97-109 (in Chinese), 2004.

25 Wang, G. H., Su, J. L., and Chu, P. C.: Mesoscale eddies in the South China Sea observed
26 with altimeter data, *Geophys. Res. Lett.*, 30, 2121, 10.1029/2003gl018532, 2003.

27 Wang, G. H., Chen, D. K., and Su, J. L.: Generation and life cycle of the dipole in the South
28 China Sea summer circulation, *J. Geophys. Res.*, 111, C06002, 10.1029/2005jc003314, 2006.

1 Xie, L. L., Tian, J. W., Zhang, S. W., Zhang, Y. W., and Yang, Q. X.: An anticyclonic eddy in
2 the intermediate layer of the Luzon Strait in Autumn 2005, *J. Oceanogr.*, 67, 37-46,
3 10.1007/s10872-011-0004-9, 2011.

4 Xiu, P., Chai, F., Shi, L., Xue, H. J., and Chao, Y.: A census of eddy activities in the South
5 China Sea during 1993-2007, *J. Geophys. Res.*, 115, C03012, 10.1029/2009jc005657, 2010.

6 You, Y. Z., Chern, C. S., Yang, Y., Liu, C. T., Liu, K. K., and Pai, S. C.: The South China
7 Sea, a cul-de-sac of North Pacific Intermediate Water, *J. Oceanogr.*, 61, 509-527, 2005.

8

9

10

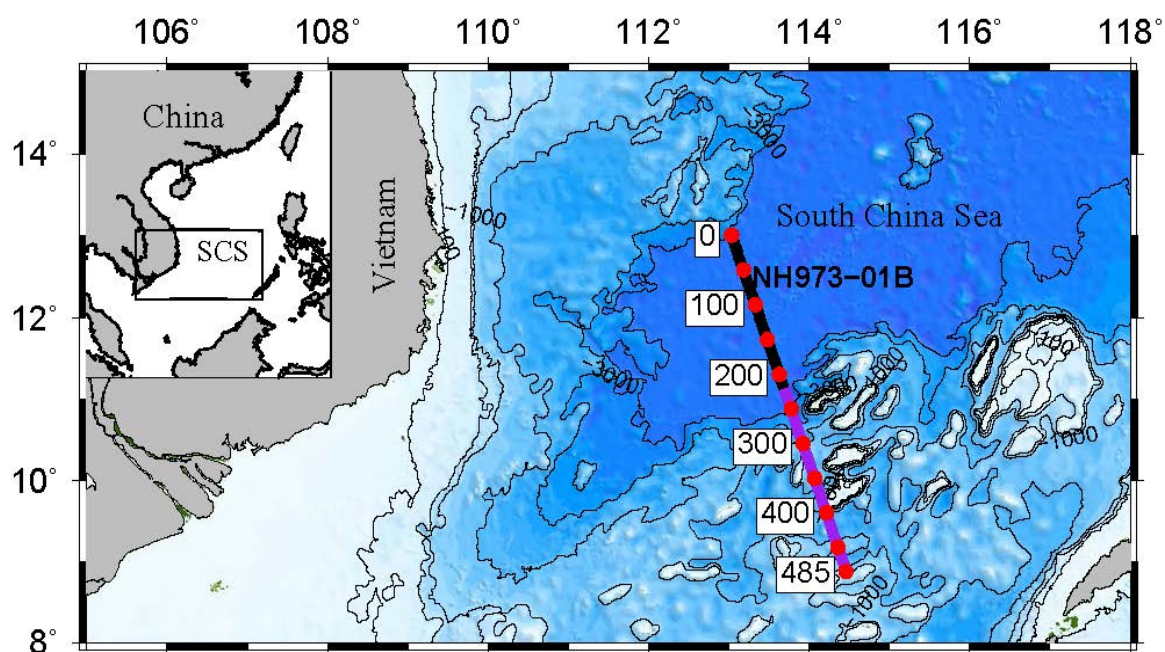


Figure 1. Bathymetry of the southern South China Sea. The seismic line NH973-01B, labelled with distances (in unit of km) from the starting point, is divided into two subsections. There is a time gap of 9 hours at the line junction.

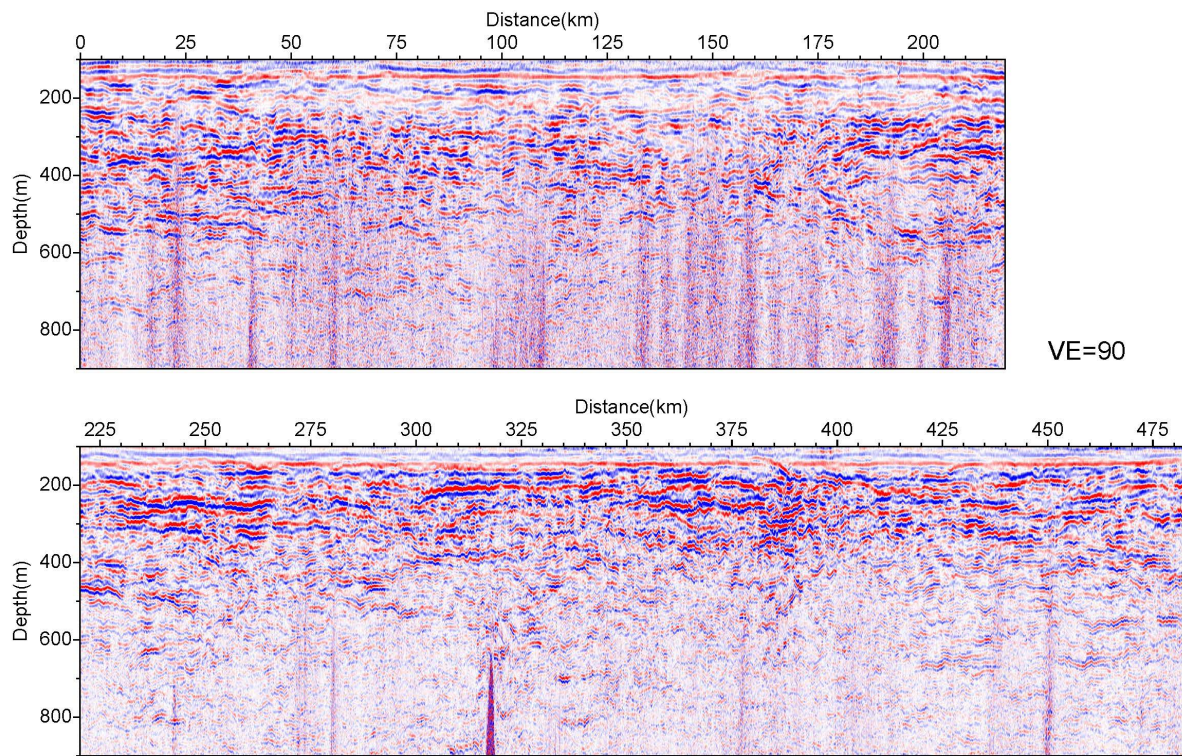


Figure 2. Seismic images of the north (upper panel) and south (lower panel) subsections with the vertical exaggeration (VE) of 90. The colour represents the relative reflection strength of the water column.

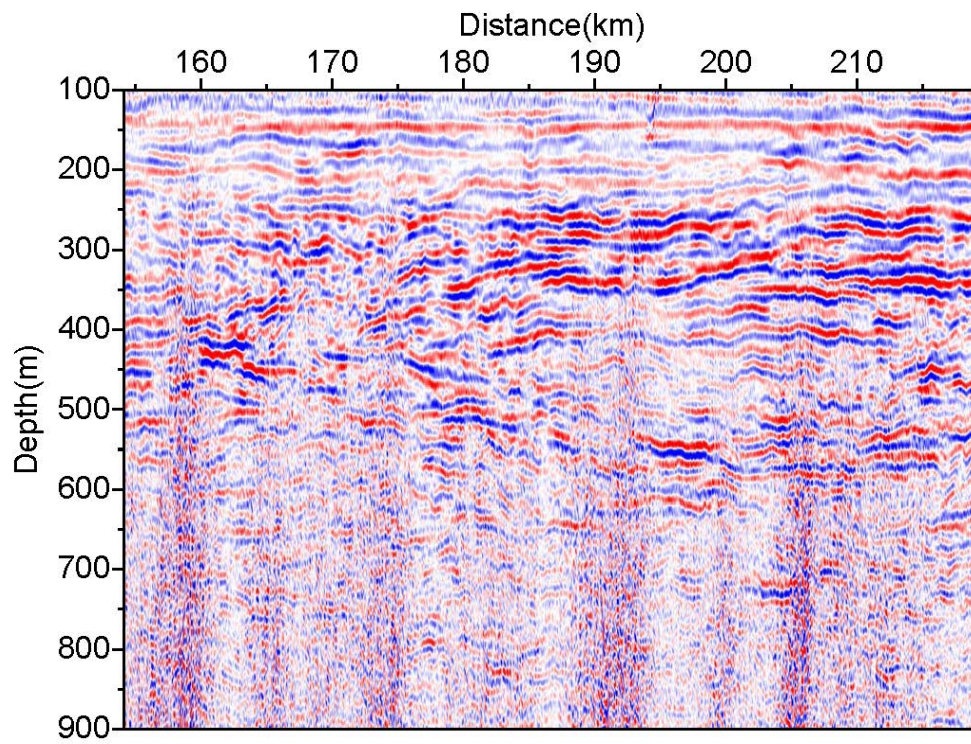


Figure 3. Detail of the subsurface eddy at the end of north subsection shown in Fig. 2. VE=60.

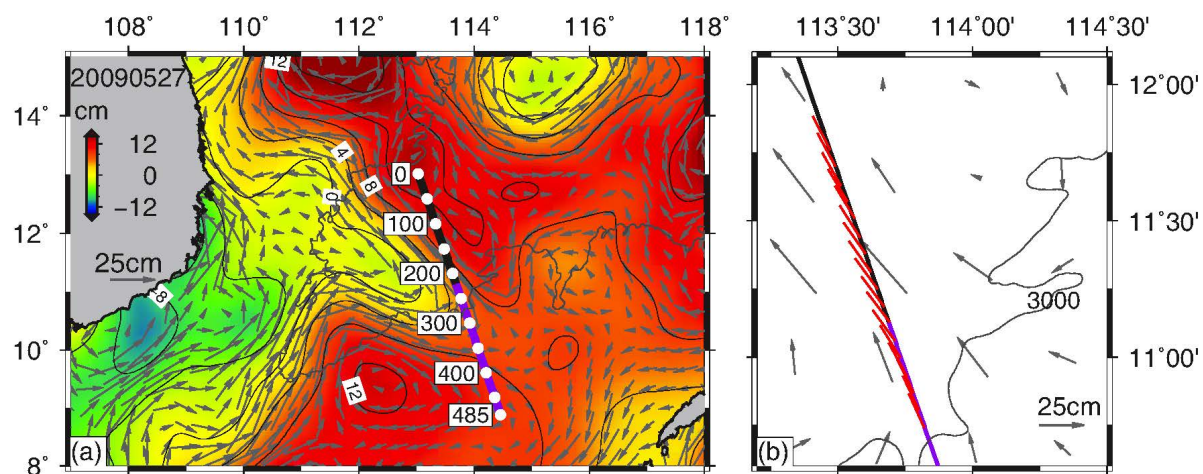


Figure 4. (a) The SLA and the corresponding surface geostrophic currents on 27 May 2009. The seismic line and the 3000-m isobath are superimposed for reference. (b) Streamer feathering (red bars) due to the strong NW current (grey arrows) around the line junction.

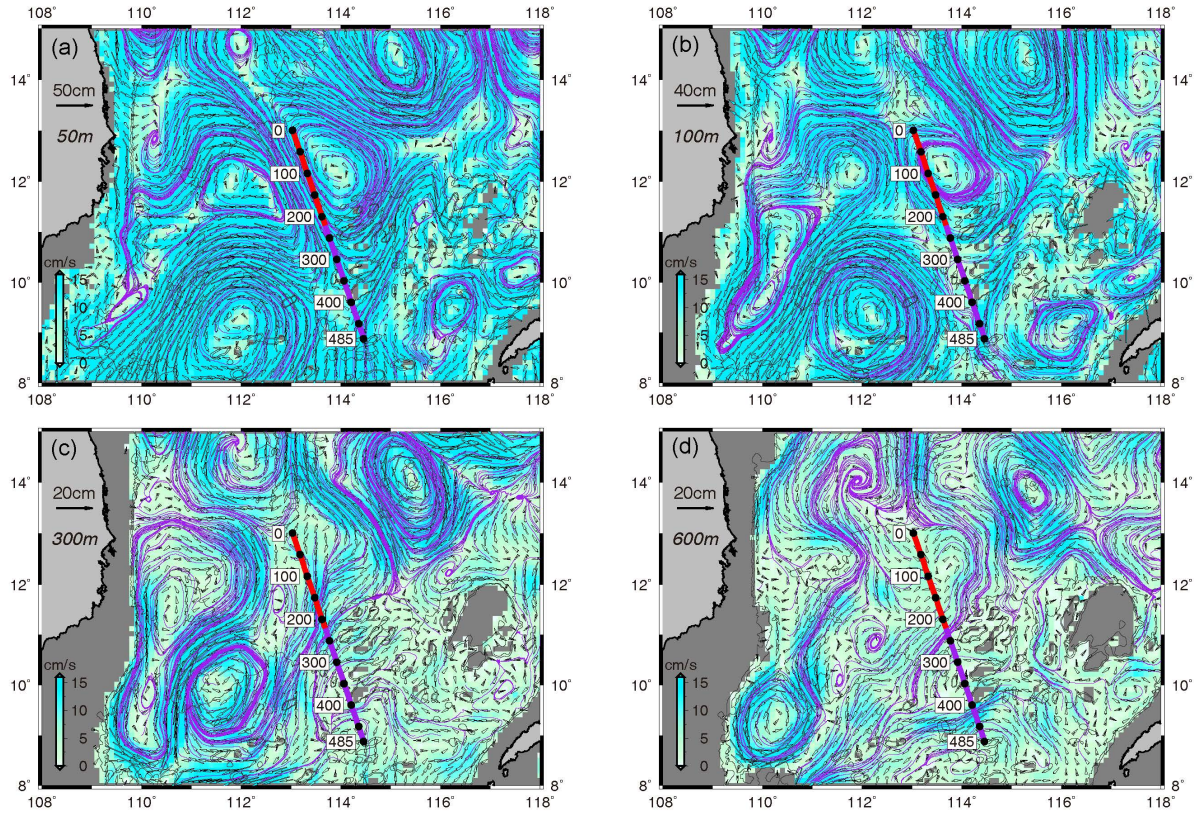


Figure 5. HYCOM simulated velocities at different depths in the southern SCS on 30 May 2009. The purple lines are the streamlines derived from the velocities. The seismic transect with labelled distances are also superimposed.

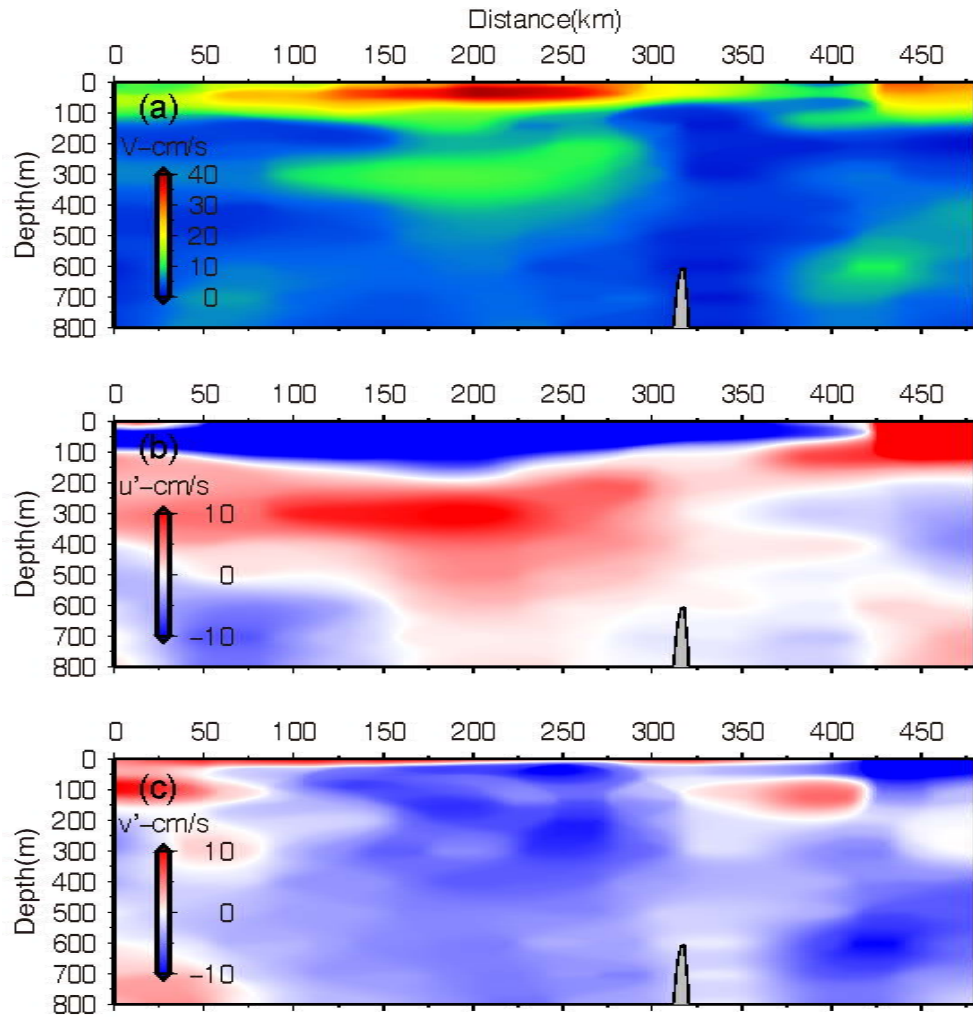


Figure 6. Vertical structures of the current speeds (a) and velocities (b and c) along the seismic transect. Where (b) and (c) show the u' and v' velocity components along and normal to the transect with positive directions being SE and NE, respectively.

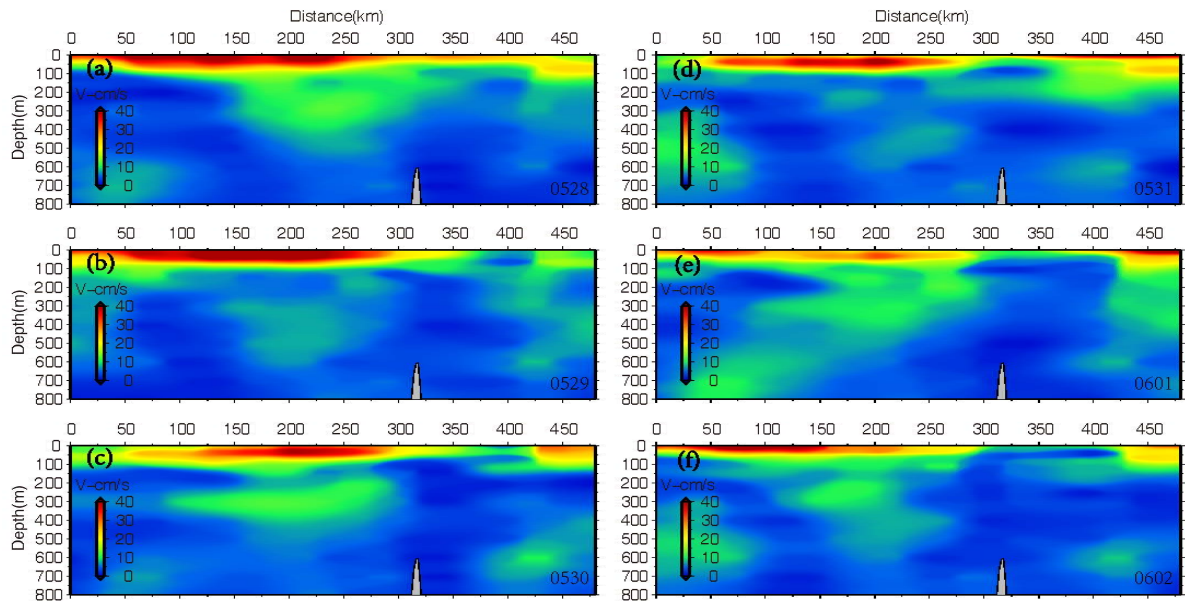


Figure 7. Daily speeds of the HYCOM results along the transect from 28 May to 2 June 2009.